





High-power, high-spectral-purity GaSb-based laterally coupled distributed feedback lasers with metal gratings emitting at $2\mu\text{m}$

Cite as: Appl. Phys. Lett. **114**, 021102 (2019); <https://doi.org/10.1063/1.5080266>

Submitted: 06 November 2018 . Accepted: 02 January 2019 . Published Online: 15 January 2019

Cheng-Ao Yang , Sheng-Wen Xie , Yi Zhang, Jin-Ming Shang, Shu-Shan Huang, Ye Yuan, Fu-Hui Shao , Yu Zhang, Ying-Qiang Xu, and Zhi-Chuan Niu 



View Online



Export Citation



CrossMark



Measure Ready
M91 FastHall™ Controller

A revolutionary new instrument
for complete Hall analysis

 Lake Shore
CRYOTRONICS

High-power, high-spectral-purity GaSb-based laterally coupled distributed feedback lasers with metal gratings emitting at $2\ \mu\text{m}$

Cite as: Appl. Phys. Lett. **114**, 021102 (2019); doi: [10.1063/1.5080266](https://doi.org/10.1063/1.5080266)

Submitted: 06 November 2018 · Accepted: 02 January 2019 · Published Online: 15 January 2019







View Online



Export Citation



CrossMark

Cheng-Ao Yang,^{1,2,3}  Sheng-Wen Xie,^{1,2,3}  Yi Zhang,^{1,2,3} Jin-Ming Shang,^{1,2,3} Shu-Shan Huang,^{1,2,3} Ye Yuan,^{1,2,3} Fu-Hui Shao,^{1,2,3}  Yu Zhang,^{1,2,3} Ying-Qiang Xu,^{1,2,3} and Zhi-Chuan Niu^{1,2,3,a)} 

AFFILIATIONS

¹ State Key Laboratory for Superlattices and Microstructures, Institute of Semiconductors, Chinese Academy of Sciences, Beijing 100083, China

² College of Materials Science and Opto-Electronic Technology, University of Chinese Academy of Sciences, Beijing 100049, China

³ Center of Materials Science and Optoelectronics Engineering, University of Chinese Academy of Sciences, Beijing 100049, China

^{a)} Author to whom correspondence should be addressed: zcniu@semi.ac.cn

ABSTRACT

We report on the fabrication of high-power, high-spectral-purity GaSb-based laterally coupled distributed feedback (LC-DFB) lasers emitting at $2\ \mu\text{m}$. Second-order Chromium-Bragg-gratings are fabricated alongside the ridge waveguide by lift off. Due to the introduction of gain coupling, the lasers exhibit a stable single mode operation [side-mode suppression ratio (SMSR) $>40\ \text{dB}$] from $10\ ^\circ\text{C}$ to $50\ ^\circ\text{C}$ and the maximum SMSR is as high as $53\ \text{dB}$. At a heat-sink temperature of $10\ ^\circ\text{C}$, the lasers emit more than $40\ \text{mW}$ continuous-wave in a single longitudinal mode. A high external quantum efficiency of 48% is obtained, resulting in a notable increase in power conversion efficiency peaking at 13% . The lasers achieve a comparable output power with that of the index-coupled LC-DFB lasers, while maintaining a better single mode performance. Thus, we prove the feasibility of the metal-grating LC-DFB structure to achieve high-power, frequency-stable semiconductor lasers through a simpler and much more convenient way.

Published under license by AIP Publishing. <https://doi.org/10.1063/1.5080266>

Semiconductor laser diodes operating in the mid-infrared ($2\text{--}4\ \mu\text{m}$) region are attractive light sources for a variety of applications, such as gas detection,¹ remote sensing,² and laser spectroscopy.³ When designing satellite-borne lidar systems based on laser absorption spectroscopy, the wavelength around $2\ \mu\text{m}$ is irreplaceable due to the strong characteristic absorption of greenhouse gases and minimal sensitivity to variations in temperature and water concentration.² Thus, both the European Space Agency and the National Aeronautic Space Administration put forward further demands on single-mode seed laser transmitters emitting around $2\ \mu\text{m}$.⁴ For continuous global-scale detection of CO_2 and other atmospheric greenhouse gases, the power of the seed lasers needs to be at least tens of milliwatts.² Taking advantages of the compactness and reliability, semiconductor lasers based on InP and GaSb are particularly suitable for aerospace systems. However, the output power of state-of-art InP-based laser diodes with single mode operation is limited to

$10\ \text{mW}$.⁵ GaSb alloys are the most promising material systems for $2\text{--}\mu\text{m}$ lasers.^{1,2} But typical lasers contains a high content of aluminum in the epitaxy layer. The oxidation of aluminum contents makes the conventional fabrication of distributed feedback (DFB) lasers with a regrowth step technically challenging. An alternative approach is placing the Bragg gratings alongside the ridge-waveguide to form a laterally coupled distributed feedback (LC-DFB) laser,⁶ which later becomes the mainstream technical solution for achieving single mode lasers on GaSb alloys.^{7–12}

To date, the leading result of high-power, single-mode semiconductor laser diodes emitting around $2\ \mu\text{m}$ is achieved by index-coupled LC-DFB (IC-LC-DFB) lasers.^{5,8,13} The maximum output power is in excess of $40\ \text{mW}$ at $10\ ^\circ\text{C}$ and $80\ \text{mW}$ at $-10\ ^\circ\text{C}$.⁵ The line width has also been compressed to the order of sub-kHz.^{14,15} However, the reported side-mode suppression ratio (SMSR) drops to $20\ \text{dB}$ – $30\ \text{dB}$ at peak output power due to a limited DFB modulation. According to coupling theory,¹⁶ the

mode stability of IC-LC-DFB lasers is disturbed by the inherent problem that two longitudinal-modes having equal threshold gain exist on either side of the stop-band.¹⁷ Although an asymmetric facet coating or a $\lambda/4$ phase shift grating is helpful for removing mode degeneracy and ensuring single mode operation,¹⁸ the manufacture process is quite complex and device performance is still limited by the spatial hole burning (SHB) effect and the random facet phases introduced by cleaving.¹⁹ In addition, an optical isolator is obliged in system-level devices due to its sensitivity to back-reflected light, which greatly increases the volume and cost.

An alternative approach is introducing gain coupling using complex-coupled LC-DFB (CC-LC-DFB) lasers. The metallic Bragg gratings act as periodic absorbers for the evanescent part of the laser mode.^{20,21} It has been theoretically^{17,22–24} and experimentally^{11,12,19,25} proved that CC-LC-DFB lasers have one lasing mode exactly at the Bragg frequency and can maintain single mode operation without extra facet coating, which solves the degeneracy problem and achieves high yield. Due to the extra gain modulation, they are also less sensitive to external feedback^{26,27} and with lower wavelength chirp.^{28,29} The metallic gratings introduce a large gain and loss margin between the primary laser mode and adjacent laser mode which results in a high SMSR.³⁰ The strong feedback caused by metal gratings provides a better single mode stability but generates additional loss in the laser cavity, resulting in a low output power of 10 mW in previous works.^{11,12} The photoelectric conversion efficiency is usually around 1%–2%. In consideration of these advantages over IC-LC-DFB lasers, CC-LC-DFB lasers are a good alternative for space-borne systems as long as increasing the output power to dozens of milliwatts.

In this work, we report on high-power, high-spectral-purity 2- μm LC-DFB lasers with metal gratings. With an increased coupling coefficient and an optimal cavity length through laser structure designs, the lasers achieve high output power with a high SMSR. The maximum output power is 40 mW per facet at 10 °C without facet coating, which is three to four times that reported in the previous works.^{11,12} The maximum SMSR achieves up to 53 dB, which is much higher than reported values.^{5,8,11,12} Due to the extra gain modulation, the laser operates without mode hopping from 10 °C to 50 °C and the SMSR remains as high as 43 dB at the maximum output power. For a short cavity length of 1 mm, the slope efficiency is increased to 0.15 W/A with a high photoelectric conversion efficiency ranging from 8.1% to 13%. Our device shows a comparable output power with the reported high-power IC-LC-DFB lasers while obtaining a better single mode performance. Complete laser performance measurements are carried out including the beam quality, line width, and temperature characteristic, rendering them well adaptable to trace-gas absorption spectroscopy and lidar systems.

The laser heterostructures were grown on an N-type GaSb (1 0 0) substrate with a 1.5 μm -thick $\text{Al}_{0.55}\text{Ga}_{0.45}\text{As}_{0.02}\text{Sb}_{0.98}$ cladding layer and a 300 nm-thick undoped $\text{Al}_{0.3}\text{Ga}_{0.7}\text{As}_{0.07}\text{Sb}_{0.93}$ waveguide layer by solid-source molecular beam epitaxy (MBE). Two pairs of 9 nm-thick $\text{In}_{0.22}\text{Ga}_{0.78}\text{As}_{0.1}\text{Sb}_{0.9}$ quantum wells centered in the waveguide layer. A linear graded layer was located between the cladding layer and the waveguide to reduce extra

light loss. The detailed information of the energy band diagram can be found in Fig. 1.

The design of our LC-DFB lasers was based on coupling theory.¹⁶ The modal effective refractive index of the unperturbed ridge laser was estimated as 3.54 using a full-vector finite-difference calculation. The feedback effect of lateral gratings can be quantified by estimating the grating coupling coefficient κ . For realizing single mode lasers, the coupling intensity κL (L : cavity length) is usually around 1–2. The Bragg gratings of CC-LC-DFB lasers interact with the evanescent part of the laser mode, resulting in a relatively small coupling coefficient κ . Thus, a longer cavity length is obliged to ensure single mode operation, which leads to a decrease in slope efficiency. Hence, there exists an optimized coupling intensity and cavity length to achieve both high output power and good single-mode operation. The coupling coefficient κ is given by³

$$\kappa = \frac{n_1^2 - n_2^2}{n_{\text{eff}} \lambda} \frac{\sin(m\pi g)}{m} \Gamma_{\text{grating}}, \quad (1)$$

where n_1 and n_2 are the complex refractive index of the grating and the covering materials, respectively, the electric-field overlap factor Γ_{grating} describes the extent to which the electric field overlaps with the grating, which is about 0.15% in our devices, g is the duty cycle of the grating, $m=2$ is the grating diffraction order, and the coupling coefficient of κ is approximately 1 mm^{-1} , resulting in a short cavity length of 1 mm to realize κL close to 1.

The ridge-waveguide was fabricated using contact lithography and etched down to a depth of 1.65 μm . Then, a 50 nm-thick Si_3N_4 layer was deposited by plasma-enhanced chemical-vapor deposition on the epitaxy for the insulation between the metal gratings and the epitaxial layer. Second-order gratings of chromium were fabricated alongside the ridge-waveguide by lift-off and covered by another Si_3N_4 layer of 250 nm. Figure 2 shows the scanning electron micrograph (SEM) of LC-DFB lasers with the inset representing detailed information of the gratings. The wafer was cleaved into 1-mm-long chips and mounted epi-side down without facet coating. The output power was measured

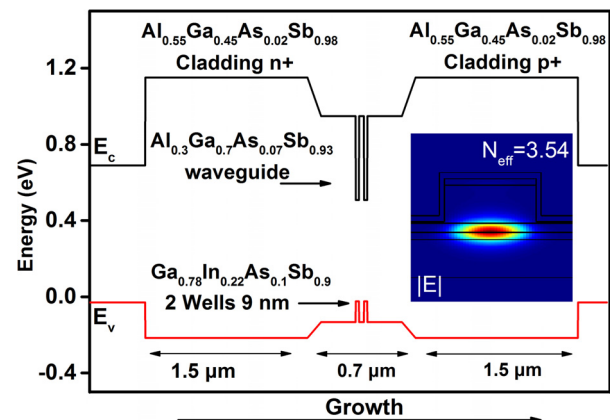


FIG. 1. Energy band diagram of the epitaxy and calculated intensity distribution of the fundamental mode (inset).

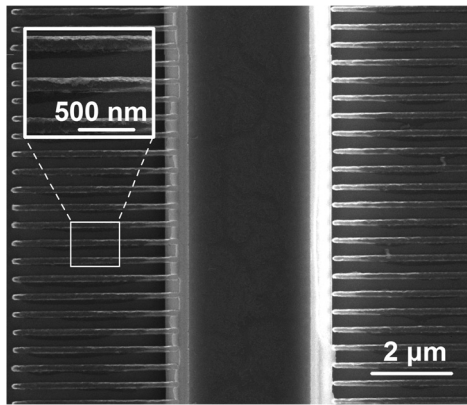


FIG. 2. Top view of the LC-DFB laser; detailed information of the grating is shown in the inset.

using a Thorlabs S401C calibrated thermopile detector. Emission spectra were obtained with a Yokogawa AQ6376 optical spectrum analyzer using multimode index fiber.

Figure 3 shows the power-current (P-I) characteristics and photoelectric conversion efficiency of the lasers with 4.5- μm -wide ridge-waveguide at different temperatures in the CW regime. The maximum output power is up to 40 mW at 10 °C per facet and remains 24 mW at 50 °C. The SMSR maintains as high as 43 dB under the peak output power as shown in Fig. 3 (inset) which is much higher than that reported in the previous works.^{5,8,11,12} The laser shows a low threshold current of 26.7 mA ($J_{\text{th}} = 593 \text{ A/cm}^2$) seen in Fig. 4 (inset), which is almost half of the reported value.^{11,12} The low threshold current indicates that our design of the LC-DFB structure introduces relatively little optical loss which contributes to the increasing output power. With a calculated facet loss of 11.6 cm^{-1} , the loss introduced by the LC-DFB structure is approximately 6.5 cm^{-1} . The loss is much

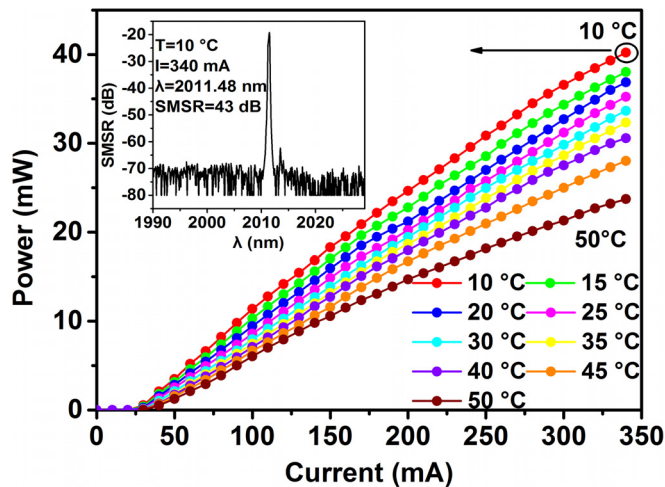


FIG. 3. CW Power-Current characteristics of a 1 mm-long-LC-DFB laser operating at different temperatures. The inset shows the laser spectrum at the maximum power output.

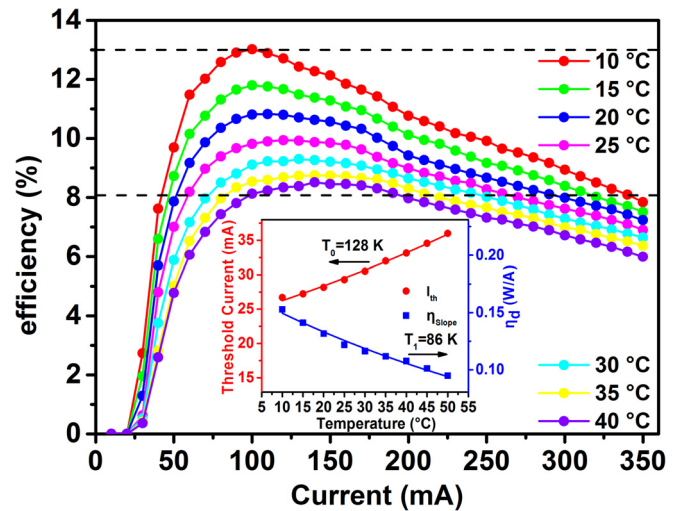


FIG. 4. The photoelectric conversion efficiency of the laser. Temperature characteristics of the laser including T_0 and T_1 .

smaller than that in the reported works and comparable with that of the IC-LC-DFB lasers based on GaSb.^{5,11,12} As is shown in Fig. 4, the total power conversion efficiency reaches 8.1% per facet and a high slope efficiency of 0.15 W/A is obtained, which corresponds to a high external quantum efficiency of 48%. The temperature characteristic is also investigated and the coefficient of T_0 is found to be as high as 128 K which can be seen in Fig. 4 (inset).

The emission spectrum of the LC-DFB laser is plotted in Fig. 5 with the inset figure representing the spectrum obtained from the broad-area laser fabricated on the same wafer. The maximum SMSR is as high as 53 dB at a driving current of 320 mA. The lasers show a stable single mode operation from 10 °C to 50 °C. The SMSR is larger than 35 dB throughout the

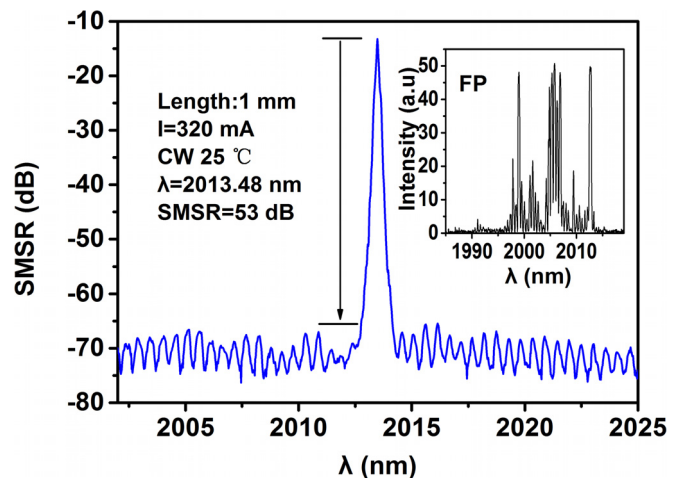


FIG. 5. The maximum SMSR of the LC-DFB laser with a driving current of 320 mA at 25 °C and the emission spectrum of a broad-area laser obtained on the same wafer.

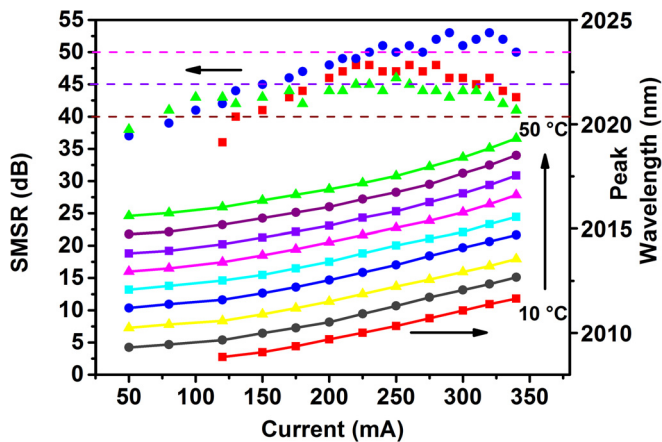


FIG. 6. Wavelength tuning against current and temperature (down). The change of SMSR with current and temperature (Up).

operation current for single mode operation. It is in excess of 40 dB and 45 dB with ratios of 90% and 54% of the working conditions, respectively. This attests to the very strong coupling of the metal grating. The SMSR varies with temperature because of the mismatch between the Bragg wavelength and the gain of the active region. The peak gain of the material drifts more rapidly than the Bragg wavelength. Thus, the SMSR increases at first and then decreases with the injection current, which can be seen in Fig. 6. Multi-mode operation becomes dominant when the driving current is beyond 340 mA. For devices with stronger coupling ($\kappa L > 1$), the single mode operation is also guaranteed but the slope efficiency decreases rapidly with the increase in coupling, which results in an obvious decline of output power. In addition, the laser oscillation is unstable and appears in multi-mode operation easily with the increasing of injection current. For under-coupled ($\kappa L < 1$) laser diodes, an obvious decrease in the SMSR is observed and single mode operation degenerates rapidly with variation of current and temperature.

As a function of current I , the DFB peak wavelength is fitted by the expression $\lambda(I) = \lambda_0 + BI + CI^2$, and the coefficients are obtained from Fig. 5 to be $\lambda_0 = 2010.81$ nm, $B = 4.44 \times 10^{-3}$ nm/mA, and $C = 2.1 \times 10^{-5}$ nm/mA², which are consistent with previous works.⁵ Our devices show a wide single mode operation ranging from 2009 nm to 2020 nm with the variation of temperature and current as is shown in Fig. 6. The drifting rate of wavelength against current and temperature is 0.0044 nm/mA and 0.19 nm/K, respectively. The emission spectra at different currents and temperatures are shown in Fig. 7. We want to emphasize that the working temperature of our device is limited by the temperature control capability of our platforms. We can deduce from the PI plot and the SMSR plot of the LC-DFB laser that our device can work with a higher temperature.

The line width of the LC-DFB laser is obtained by the Scanning Fabry-Perot interferometer with a free spectral range (FSR) of 1.5 GHz (finesse is 200) as shown in Fig. 8. The derived line width of 9 MHz, which is suitable for detection systems, is an upper bound of instrumental noise and around the measurement limit of our interferometer, indicating that the actual line

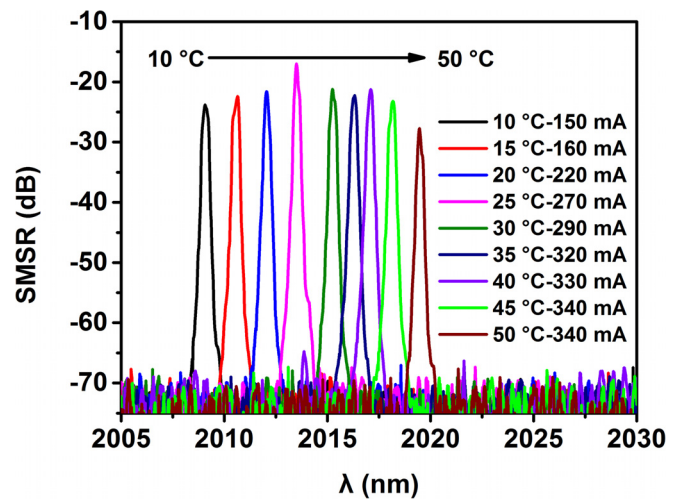


FIG. 7. Emission spectra of lasers at different driving currents and temperatures.

width is narrower. Figure 9 shows the far-field intensity distribution of the laser beam along the fast and slow axes, with an elliptical divergent beam (FWHM, $14^\circ \times 42^\circ$). The M^2 factors along the horizontal axis and vertical axis are 1.03 and 3.37, respectively. Due to a large elliptical divergent, the output beam is truncated by lens, which greatly increases the value of M^2 along the fast axis.

We have fabricated high-power, high-spectral-purity GaSb-based CC-LC-DFB lasers. Due to the introduction of complex coupling and an optimized coupling intensity, the laser diodes show a comparable output power with the leading high-power IC-LC-DFB lasers while maintaining a better single mode performance. For a 1-mm-long uncoated laser diode, the

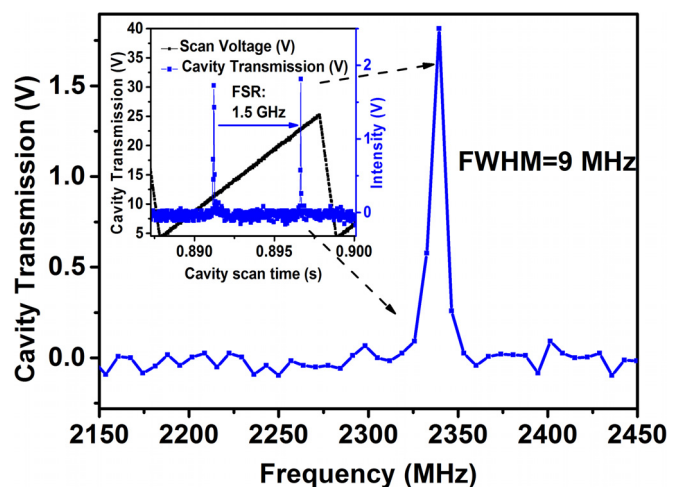


FIG. 8. Line width obtained by estimating the FWHM of the resonances of interferometer. The inset shows the FSR of the interferometer.

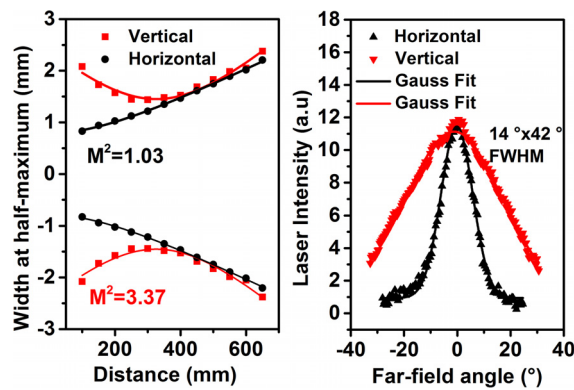


FIG. 9. Beam quality (left) and far-field intensity distribution of the laser beam along the fast and slow axes (right) of the LC-DFB lasers.

continuous-wave output power exceeds 40 mW per facet with a photoelectric conversion efficiency of 8.1% at room temperature, which is three to four times that of previous CC-LC-DFB lasers.^{11,12} The maximum SMSR achieves up to 53 dB and remains in excess of 40 dB from 10 °C to 50 °C, indicating good mode selection characteristics. These improved performances are attributed to the high quality of epitaxial, optimal device design, and good device fabrication techniques. These results prove the feasibility of the metal-grating LC-DFB structure to achieve high-power, frequency-stable semiconductor lasers with better performance and are an important step towards the realization of seed lasers suitable for airspace applications.

This work was supported by the Major Program of the National Natural Science Foundation of China (Nos. 61790580 and 61435012), the Scientific Instrument Project of the Chinese Academy of Sciences (No. YJKYQ20170032), and the National Basic Research Program of China (No. 2014CB643903). We would like to thank Dr Ying Yu and Dr Si-Hang Wei for fruitful discussions and support.

REFERENCES

- ¹R. A. Anthes and B. Moore III, *Earth Science and Applications from Space: National Imperatives for the Next Decade and Beyond* (The National Academies Press, Washington, DC, 2007).
- ²J. A. Gupta, P. J. Barrios, J. Lapointe, G. C. Aers, and C. Storey, *Appl. Phys. Lett.* **95**(4), 041104 (2009).
- ³J. A. Gupta, P. J. Barrios, J. Lapointe, G. C. Aers, C. Storey, and P. Waldron, *IEEE Photonics Technol. Lett.* **21**(20), 1532–1534 (2009).
- ⁴C. A. Yang, Y. Zhang, Y. P. Liao, J. L. Xing, S. H. Wei, L. C. Zhang, Y. Q. Xu, H. Q. Ni, and Z. C. Niu, *Chin. Phys. B* **25**(2), 024204 (2016).
- ⁵S. Forouhar, R. M. Briggs, C. Frez, K. J. Franz, and A. Ksendzov, *Appl. Phys. Lett.* **100**(3), 031107 (2012).
- ⁶Z. L. Liao, D. C. Flanders, J. N. Walpole, and N. L. DeMeo, *Appl. Phys. Lett.* **46**(3), 221 (1985).
- ⁷M. Muller, A. Bauer, T. Lehnhardt, M. Kamp, and A. Forchel, *IEEE Photonics Technol. Lett.* **20**(24), 2162–2164 (2008).
- ⁸P. Apiratikul, L. He, and C. J. K. Richardson, *Appl. Phys. Lett.* **102**(23), 231101 (2013).
- ⁹J. Viheriäla, K. Haring, S. Suomalainen, R. Koskinen, T. Niemi, and M. Guina, *IEEE Photonics Technol. Lett.* **28**(11), 1233–1236 (2016).
- ¹⁰R. M. Briggs, C. Frez, M. Bagheri, C. E. Borgentun, J. A. Gupta, M. F. Witinski, J. G. Anderson, and S. Forouhar, *Opt. Express* **21**(1), 1317–1323 (2013).
- ¹¹A. Salhi, D. Barat, D. Romanini, Y. Rouillard, A. Ouvrard, R. Werner, J. Seufert, J. Koeth, A. Vicet, and A. Garnache, *Appl. Opt.* **45**(20), 4957–4965 (2006).
- ¹²K. Rossner, M. Hummer, A. Benkert, and A. Forchel, *Physica E* **30**(1–2), 159–163 (2005).
- ¹³M. Bagheri, C. Frez, B. Kelly, J. A. Gupta, and S. Forouhar, *Electron. Lett.* **49**(24), 1552 (2013).
- ¹⁴M. Bagheri, G. D. Spiers, C. Frez, S. Forouhar, and F. Aflatouni, *IEEE Photonics Technol. Lett.* **27**(18), 1934–1937 (2015).
- ¹⁵E. Dale, M. Bagheri, A. B. Matsko, C. Frez, W. Liang, S. Forouhar, and L. Maleki, *Opt. Lett.* **41**(23), 5559–5562 (2016).
- ¹⁶H. Kogelnik, *J. Appl. Phys.* **43**(5), 2327 (1972).
- ¹⁷K. David, G. Morthier, P. Vankwikelberge, R. G. Baets, T. Wolf, and B. Borchert, *IEEE J. Quantum Electron.* **27**(6), 1714–1723 (1991).
- ¹⁸J. Buus, *Electron. Lett.* **21**(5), 179–180 (1985).
- ¹⁹S. T. Kim and B. G. Kim, *J. Opt. Soc. Am. B* **22**(5), 1010–1015 (2005).
- ²⁰H. L. Cao, Y. Luo, Y. Nakano, K. Tada, M. Dobashi, and H. Hosomatsu, *IEEE Photonics Technol. Lett.* **4**(10), 1099–1102 (1992).
- ²¹S. K. C. Liew, *IEEE Photonics Technol. Lett.* **7**(12), 1400–1402 (1995).
- ²²B. Borchert, K. David, B. Stegmüller, R. Gessner, M. Beschoner, D. Sacher, and G. Franz, *IEEE Photonics Technol. Lett.* **3**(11), 955–957 (1991).
- ²³G. P. Li, T. Makino, R. Moore, N. Puetz, K. Leong, and H. Lu, *IEEE J. Quantum Electron.* **29**(6), 1736–1742 (1993).
- ²⁴Y. Nakano, Y. Ushida, and K. Tada, *IEEE Photonics Technol. Lett.* **4**(4), 308–311 (1992).
- ²⁵C. Yang, S. Xie, S. Huang, Y. Yuan, Y. Zhang, J. Shang, Y. Zhang, Y. Xu, and Z. Niu, “High-power laterally-coupled distributed feedback lasers with metal gratings around 2 μm,” *IEEE Photonics Technol. Lett.* (published online).
- ²⁶R. Hui, M. Kavehrad, and T. Makino, *IEEE Photonics Technol. Lett.* **6**(8), 897–899 (1994).
- ²⁷C. Zhang, S. Liang, H. Zhu, L. Han, and W. Wang, *IEEE J. Quantum Electron.* **50**(2), 92–97 (2014).
- ²⁸A. J. Lowery and D. Novak, *Electron. Lett.* **29**(5), 461–463 (1993).
- ²⁹Y. Xi, W. Huang, and X. Li, *J. Lightwave Technol.* **27**(17), 3853–3860 (2009).
- ³⁰K. David, J. Buus, and R. G. Baets, *IEEE J. Quantum Electron.* **28**(2), 427–434 (1992).